Feng *et al.*
Chinese Journal of Mechanical Engineering (2023) 36:122
https://doi.org/10.1186/s10033-023-00952-z

Chinese Journal of Mechanical Engineering

ORIGINAL ARTICLE

Open Access

Dynamic Simulation and Test Verification of Hydraulic Automatic Tensioner for an Engine Timing Chain Drive System

Zengming Feng[1], Jinxing Yang[1*] and Fei Wang[1]

Abstract

As a fundamental component of an automobile engine's timing chain drive system, the hydraulic automatic tensioner significantly enhances fuel economy while minimizing system vibrations and noise. However, there is a noticeable lack of research on automatic hydraulic tensioners. This study presents a comprehensive calculation approach for the principal parameters of a hydraulic automatic tensioner. An effective method, grounded in hydraulics and multibody dynamics, was introduced for estimating the dynamic response of such a tensioner. The simulation model developed for the hydraulic tensioner is characterized by its rapid dynamic response, consistent operation, and high accuracy. The dynamic behavior of the tensioner was analyzed under varying boundary conditions, using sinusoidal signal excitation. It was observed that the maximum damping force increases with a decreasing leakage gap. Conversely, an increase in oil temperature or air content leads to a decrease in the maximum damping force. The reaction forces derived from these calculations align well with experimental results. This calculation and simulation approach offers considerable value for the design of innovative hydraulic tensioners. It not only streamlines the design phase, minimizes the number of trials, and reduces product costs, but also provides robust insights for evaluating the performance of hydraulic tensioners.

Keywords Hydraulic automatic tensioner, Timing chain, Leakage gap, Hysteresis curve

1 Introduction

With the advent of novel engine technologies, such as turbochargers [1, 2] and fuel-stratified injections [3], engines are increasingly adopting timing chain systems in lieu of gear or belt systems, aiming for reduced fuel emissions. The timing chain system stands out for its zero maintenance requirements, high reliability, and life expectancy that matches that of vehicles.

Switching from belt or gear systems to the durable timing chain system enhances fuel efficiency and leads to reduced emissions. However, the timing chain system is not without challenges. Factors, such as the polygon effect, the repetitive impacts of the chain at the engagement points of guides and sprockets, inconsistencies in crankshaft rotation, and variations in camshaft torque, cause substantial transverse vibrations and slapping noises during operation. Hence, ensuring chain tension and diminishing drive noise and lateral vibration become crucial for the system's durability and reliability [4, 5]. Feng et al. addressed the polygon effect and chain drive wear by developing an internal-external compound meshing silent chain, validating it through simulation [6]. Li et al. introduced a dynamic model for the timing chain drive system, analyzing aspects like link rotation speed, chain tension, tensioner force, and variations in the intake camshaft sprocket angular velocity. This research concluded that the silent chain drive system exhibited a markedly reduced polygon effect compared

*Correspondence:
Jinxing Yang
yangjx21@mails.jlu.edu.cn
[1] School of Mechanical and Aerospace Engineering, Jilin University, Changchun 130022, China

to the sleeve chains [7]. Mulik et al. crafted a model for a timing chain drive system tailored for high-speed diesel engines and delved into chain tension and the contact force between the chain, guide rail, and sprocket [8]. Cali et al. significantly ameliorated the dynamic performance of a silent chain drive system by adjusting the meshing angle between the chain and sprocket [9]. Yang et al., using a multibody dynamics analysis, examined the transmission error, chain trajectory, and chain tension of the timing chain drive system. The study further evaluated the impact of vital parameters like sprocket speed, oil injection volume, lubricant viscosity, and injection angle on the system's lubrication efficiency [10]. Collectively, these studies have advanced the understanding and optimization of the timing chain system by exploring its meshing mechanisms and utilizing multibody dynamics simulations.

Over extended periods of operation, the timing chain undergoes elongation, and this elongation intensifies as sprocket speed increases. Excessive elongation can give rise to issues such as tooth skipping and chain slackening, both of which compromise the system's transmission precision and efficiency. Within this system, the tensioner holds significant importance. As the chain elongates, the tensioner's plunger extends due to hydraulic pressure to offset this elongation. This adjustment curtails chain fluctuations and transmission noise, ensuring the steady functioning of the chain-drive-timing system.

Tensioners are frequently employed to diminish transverse vibrations in flexible drive systems. Kraver et al. conducted a comprehensive model analysis to assess the impact of tensioner spring rigidity and dry friction damping on the dynamic traits of a V-belt attachment drive system [11]. Michon et al. developed a model capturing the hysteretic behavior of belt tensioners and ascertained the model's preloads, forcing frequencies, and deflection magnitudes through experiments, noting that the system's response surged with both excitation frequency and amplitude [12]. Chen et al. utilized an adaptive control approach to apply torque to a tensioner arm, thereby reducing the transverse vibration of the controlled span [13]. Podsiedlik et al. introduced a multibarrier electromagnetic tensioner. Its magnetic circuit ensures automatic adaptation to yarn tension variations, diminishes frictional losses in the guidance system, and boosts the system's operational precision [14]. Takagishi et al. constructed an exhaustive chain drive dynamic model and deduced that, in comparison to the spring tensioner, the hydraulic variant is more adept at handling load variations and curbing the chain's transverse vibrations [15]. Hu et al. delved into the damping attributes of a hydraulic automatic tensioner piston in an engine accessory wheel train, employing both numerical solutions and finite element simulations for analysis when stimulated by a straightforward harmonic displacement [16]. Zeng et al. formulated a hysteresis loop model detailing the torque-angular displacement dynamics of the tensioner within the engine's front-end accessory drive system. This model considered factors like the tensioner's preload torque, spring stiffness, damping coefficient, and the tensioner arm's moment of inertia, with experimental validations confirming its accuracy [17]. Xi et al. aimed to lower the vibration noise in a chain drive system by enhancing the hydraulic tensioner's damping features [18]. Although tensioners find usage across various applications, studies specifically focusing on their role in chain drives remain limited.

In the timing chain system, the tensioner typically serves as the pivotal component to mitigate chain tension and vibration noise. A prominent example of such a tensioner is the hydraulic automatic tensioner, which boasts a robust damping force to counter chain fluctuations. The chain load is absorbed through the optimal damping generated by the synergy between hydraulic and mechanical interconnections. This paper presents a comprehensive method for calculating the essential parameters of the hydraulic tensioner. It also delves into the characteristics of the hydraulic tensioner's damping force under varied boundary conditions, including leakage gap, oil temperature, and air content. The machine–hydraulic co-simulation technology facilitates not only the simulation of the system's multibody dynamic performance but also the exploration of the tensioner's nonlinear attributes.

2 Operating Principle of Hydraulic Automatic Tensioner

2.1 Structure of Hydraulic Automatic Tensioner

Figure 1 illustrates the structure of the hydraulic tensioner. Its primary components include the housing, a check valve affixed to the oil supply line, plunger, plunger

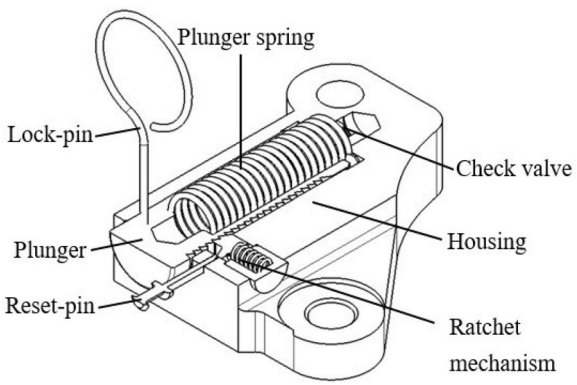

Figure 1 Hydraulic tensioner

spring, a lock-pin that restricts plunger movement, reset-pin, and ratchet mechanisms. The high-pressure chamber is encased by the housing and plunger. Oil is channeled to the tensioner from the pump via the engine's oil supply lines. The initial tension force is established by the combined load from oil pressure and the main spring. The minimal preload applied on the chain by the hydraulic tensioner is dictated by the valve assembly parameters and chain mass [19]. During its operation, the hydraulic tensioner undergoes two primary phases: compression and expansion. In the expansion phase, the check valve is activated, allowing oil from the supply line to fill the chamber. Subsequently, the force generated by the oil pressure combined with the spring propels the plunger outward. In contrast, during the compression and damping phases, the plunger is drawn inward, and the check valve shuts, preventing the oil from retreating back to the supply line. The oil accumulated within the chamber is then discharged from the tensioner through either the leakage gap or a relief valve, serving the dual purpose of safeguarding and lubricating the timing chain drive system. Concurrently, the tensioner generates a substantial damping force to counteract the chain's transverse vibrations. It's imperative that the damping force rendered by the hydraulic tensioner remains consistent throughout each operational cycle to effectively combat chain transverse vibrations and regulate chain tension.

2.2 Plunger Motion Equation

The structural diagram of the plunger is shown in Figure 2, where the plunger force produced by the tensioner is transferred to the moving guide to counteract the fluctuation in the timing chain drive. Hydraulic and mechanical interconnections commonly result in plunger motion. Consequently, the plunger operates based on the load balance, as indicated in Eq. (1):

$$m_P\ddot{X}_P = K_P(X_{P0} - X_P) + (P_c - P_a)\frac{\pi d_P^2}{4} - F - F_g, \tag{1}$$

where m_p denotes the plunger mass, X_p denotes the plunger displacement, and P_c denotes the oil pressure in the high-pressure chamber. Furthermore, P_a denotes the external environmental pressure on the plunger, d_p denotes diameter of the plunger, F denotes the load applied to the plunger, K_p denotes the spring coefficient, X_{p0} denotes the initial compression length of the spring, and F_g denotes the gravity. Compared to the dynamic force, the influence of gravity is comparatively small but can be described as F_g when required [20].

2.3 Motion Equation of Check Valve

Figure 3 shows a diagram of the check valve structure. The diagram shows that the check ball is governed by the oil pressure and check valve spring. Therefore, the check ball motion was determined using Eq. (2):

$$m_B\ddot{X}_B = -K_sX_B - C_S\dot{X}_B - F_s + A_B(P_e - P_c), \tag{2}$$

where m_B denotes the check ball mass, and X_B denotes the displacement of the check ball. Furthermore, C_S denotes the damping coefficient, K_S denotes the spring coefficient, F_S denotes the initial spring force, A_B denotes the cross-sectional area of the check ball, P_e denotes the oil supply pressure on the check ball, and P_c denotes the chamber pressure.

2.4 Oil Flow Rate Through the Check Valve

The oil pump began to supply oil to the tensioner along the oil supply lines when the engine was operated. As shown in Figure 4, the theoretical flow of oil into the tensioner is calculated using Eqs. (3) and (4) [21] as follows:

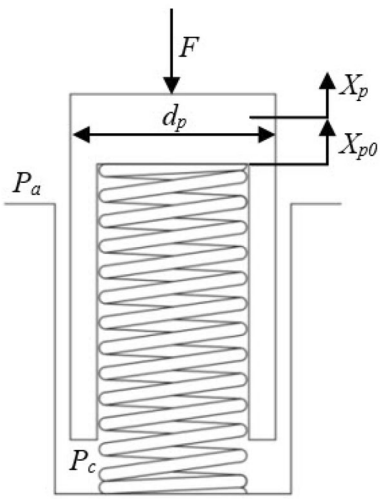

Figure 2 Structural diagram of the plunger

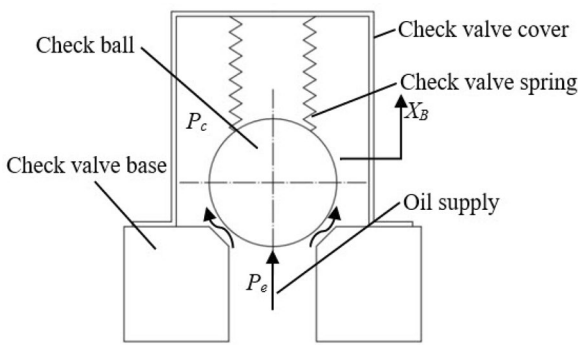

Figure 3 Structural diagram of the check valve

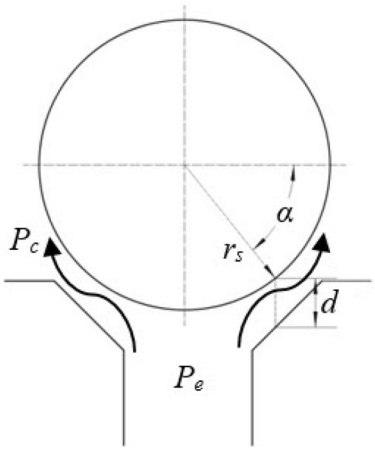

Figure 4 Oil flows through check valve

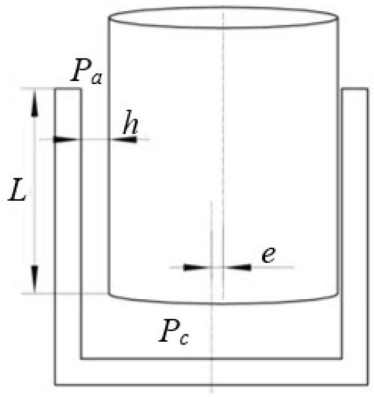

Figure 5 Leakage gap diagram

if $P_e > P_c$,

$$Q_{\text{supply}} = C_d \cdot A \cdot \sqrt{\frac{2}{\rho}(P_e - P_c)}, \tag{3}$$

if $P_e < P_c$,

$$Q_{\text{supply}} = 0, \tag{4}$$

where Q_{supply} denotes the oil flow rate through the check valve, C_d denotes the discharge coefficient of the check valve, and ρ denotes the hydraulic oil density. The flow area A for the check valve was the envelope area of the truncated cone.

$$A = \pi d \sin\alpha \cos\alpha (2r_s + d \sin\alpha), \tag{5}$$

where α denotes the angle, r_s denotes the check ball radius, d denotes the distance between the check ball and check valve base.

2.5 Leakage Gap

The leakage gap plays a pivotal role in the hydraulic tensioner's function, crucial for minimizing vibration and noise. It also significantly impacts the dynamic performance of the tensioner. When the leakage gap is utilized appropriately, the hydraulic tensioner can generate the necessary damping to offset the chain load. A larger leakage gap results in reduced damping force, compromising the tensioner's effectiveness in maintaining chain tension. This scenario tends to produce noise and vibrations in the chain drive system. Conversely, an exceedingly narrow leakage gap can produce an immense reaction force in the plunger upon excitation, causing the chain's tension to surpass permissible levels, which in turn considerably diminishes the chain's lifespan. As such, the dynamic characteristics of the hydraulic tensioner are intimately tied to the size of the leakage gap, underscoring the importance of analyzing its influence on the hydraulic system. Under the assumption of laminar flow and that the flow is solely directed towards the leakage. According to the established physical model, the leakage rate corresponds to the flow passing through the leakage gap between the cylinder and plunger. However, if the tensioner is equipped with a relief valve, then both the flow through this valve and the leakage gap require calculation. If the plunger has offsets relative to the cylinder, then the effect of these offsets on the leakage flows should be considered. As shown in Figure 5, in terms of the plunger with offsets related to cylinder, the coefficient $\alpha_{\Delta P}$ is calculated in Eq. (6).

$$\alpha_{\Delta P} = -\frac{\pi d_p h^3}{12\mu L}\left(1 + 1.5\frac{e^2}{2h^2}\right), \tag{6}$$

where e denotes the relative deflection at the concentric position, h denotes the height of the leakage gap, μ denotes oil kinematic viscosity, and L denotes the leakage gap length.

The oil flowing through the leakage gap mainly depends on the difference between the chamber pressure and external environmental pressure. Consequently, the flows through the leakage gap are:

$$Q_{\text{leakage}} = \alpha_{\Delta P}(P_c - P_a). \tag{7}$$

2.6 Bulk Modulus

The bulk modulus plays a crucial role in influencing hydraulic systems. Factors such as oil temperature, pressure, air content, and oil type can affect it. Typically, an uptick in air content elevates the compression ratio of the hydraulic medium, resulting in a notable decrease in the bulk modulus. Conversely, an increase in oil pressure

and temperature tends to enhance the bulk modulus. This change directly impacts both the natural frequency and the damping ratio. When compressed, the viscous medium generates a specific elastic force, displaying elastic potential. This process can result in suboptimal damping characteristics. As such, oil compressibility can influence the energy efficiency of the hydraulic automatic tensioner. Given that the compression ratio of the viscous medium can fluctuate based on external pressure and air content shifts, the stiffness of a tensioner due to oil compressibility exhibits dynamic variability. This change markedly affects the effective driving force, stability, and the hydraulic system's dynamic response [22]. The bulk modulus of the hydraulic oil, represented as E, is detailed as follows:

$$E = -\frac{V}{\dot{V}}\dot{P}, \tag{8}$$

where V denotes the volume of the high-pressure chamber, $\dot{V}$ denotes change ratio of the volume, and $\dot{P}$ denotes change ratio of the pressure. The working oil consists of pure hydraulic oil and air. Under pressure, some air content dissolves in the hydraulic oil, while the rest remains suspended as free air bubbles within the oil. When air is dissolved in the hydraulic oil, it greatly influences the oil's compressibility, leading to a marked reduction in damping capacity, especially when exposed to lower amplitude and frequency excitations. Since dissolved air doesn't alter the oil's physical properties, the effective bulk modulus encompasses the bulk moduli of both the pure hydraulic oil and the air bubbles. Consequently, the combined elastic modulus, represented as E_{Res}, is defined as follows:

$$E_{Res} = \frac{1}{\frac{1-r_{air}}{E_{oil}} - \frac{r_{air}}{E_{air}}}, \tag{9}$$

where r_{air} denotes the air ratio in oil, E_{oil} denotes the pure oil bulk modulus, and E_{air} denotes the bulk modulus of the air bubbles.

In the isothermal case, assume that bulk modulus of air can be formulated as:

$$E_{air} = P. \tag{10}$$

In the isentropic case, assume that bulk modulus of air can be formulated as:

$$E_{air} = \frac{C_P}{C_V}P, \tag{11}$$

where C_P/C_V denotes the ratio of the isobaric specific heat capacity to the constant-volume specific heat capacity. Furthermore, with respect to air, the following holds:

$$E_{air} = 1.4P. \tag{12}$$

The pure oil bulk modulus formula is as follows:

$$E_{oil} = E_{oil0} + c(P - P_0), \tag{13}$$

where c denotes the pressure coefficient; E_{oil0} denotes the bulk oil modulus when the initial pressure is P_0; and P denotes the working pressure. The air volume in the hydraulic oil is different because the pressure and temperature of the oil change [23]:

$$V_{air} = (\frac{P_0}{P})^{1/k} \cdot V_{air0}, \tag{14}$$

where k denotes the specific heat, and V_{air0} denotes the initial air volume. The hydraulic oil volume is calculated as follows:

if $c \neq 0$,

$$V_{oil} = \frac{(1 - r_{air0})\ V_0}{\left(\frac{E_{oil}}{E_{oil0}}\right)^{1/c}}, \tag{15}$$

if $c = 0$,

$$V_{oil} = \frac{(1 - r_{air0})\ V_0}{e^{(\frac{P-P_0}{E_{oil0}})}}. \tag{16}$$

Therefore, the ratio of air content is follows:

$$r_{air} = \frac{V_{air}}{V_{air} + V_{oil}}. \tag{17}$$

The calculated values of V_{oil}, V_{air}, and r_{air} from the above formulas were substituted into Eq. (9). Hence, it can obtain the bulk modulus of mixture E_{Res}.

2.7 Volume and Pressure in the High-pressure Chamber

The volume change in the high-pressure chamber was mainly due to the motion of the plunger.

$$V_c = V_{c0} + \frac{\pi d_p^2}{4}X_P, \tag{18}$$

where V_{c0} denotes the initial volume of the high-pressure chamber. The fluid volume change rate is due to the difference between the inflow and outflow of the fluid and the change ratio of the chamber volume:

$$\dot{V} = -\frac{\pi d_p^2}{4}\dot{X}_p + Q_{\text{supply}} - Q_{\text{leakage}}. \tag{19}$$

As described above, the pressure of high-pressure chamber is calculated as follows:

$$\dot{P}_c = -E_{\mathrm{Res}} \frac{-\frac{\pi d_p^2}{4}\dot{X}_p + Q_{\mathrm{supply}} - Q_{leakage}}{V_c}. \quad (20)$$

When the oil supply pressure is constant, the pressure of the high-pressure chamber is inversely proportional to the initial volume of the high-pressure chamber. It is necessary to consider the influence of the initial volume in the high-pressure chamber on the damping characteristics of the tensioner.

2.8 Force Boundary

To guarantee that the maximum tension of the timing chain remains below the fatigue breaking load, the maximum damping force of the hydraulic tensioner must be controlled. The breaking load of the timing chain at its maximum speed was derived from a rotary fatigue test of the chain. In the timing chain drive system (as depicted in Figure 6), the relationship between the slack side chain tension, F_s, and tensioner plunger force, F_r, is as follows:

$$F_r = \frac{F_c L_t}{L} = \frac{2F_s L_t \cos\theta}{L}, \quad (21)$$

where F_c denotes the slack-side resultant force, θ denotes the angle between the chain tension on the slack side and the resultant force, L_t denotes the force arm of the resultant force of the slack-side chain tension, and L denotes the force arm of the tensioner reaction force.

The fatigue breaking load of the chain dictates the maximum damping force of the hydraulic tensioner.

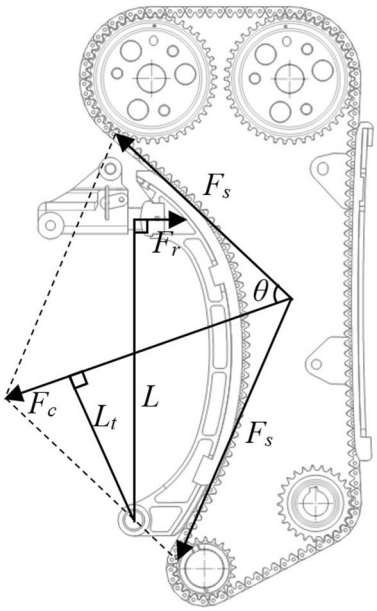

Figure 6 Moment balance relationship between chain tension and plunger reaction force

This damping force represents the peak force exerted by the hydraulic tensioner on the timing guide. Hence, it is imperative to ensure that the designed reaction force of the hydraulic tensioner consistently remains below the maximum permissible force under specific excitation conditions. Using the calculated maximum reaction force as a reference, the size of the hydraulic tensioner's leakage gap can initially be determined, either based on prior experience or through dynamic analysis.

3 Research on Dynamic Characteristics of Hydraulic Tensioner

3.1 Simulation Model

Through the establishment of a combined motion equation, the reaction force and chamber pressure, indicative of the hydraulic tensioner's dynamic performance, are derived. By accounting for the movement of all mechanical parts and the flow of the hydraulic medium within the hydraulic tensioner, a comprehensive model of the tensioner is formulated mathematically. Figure 7 illustrates a dynamic model of the hydraulic tensioner crafted using RecurDyn. The pivotal parameters of the tensioner model are presented in Table 1. Figure 8 depicts a sinusoidal

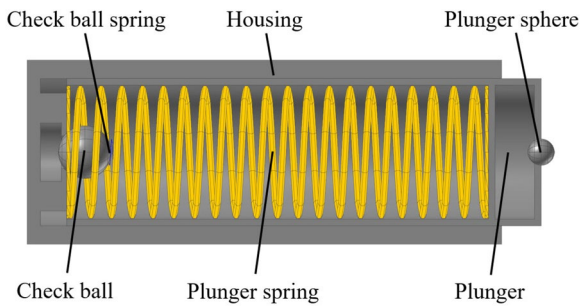

Figure 7 Dynamic model of hydraulic tensioner

Table 1 Structure parameters of the hydraulic tensioner

Features	Value
Inner radius of the plunger(mm)	4
Outer radius of the plunger(mm)	5
Initial chamber volume(mm^3)	392.7
Stiffness retainer spring(N/mm)	1
Preload retainer spring(N)	20
Average leakage gap(mm)	0.035
Leakage length(mm)	30
Radius of the ball(mm)	2
Value seat diameter(mm)	2.5
Max. ball lift(mm)	0.5
Mass of ball(g)	0.2

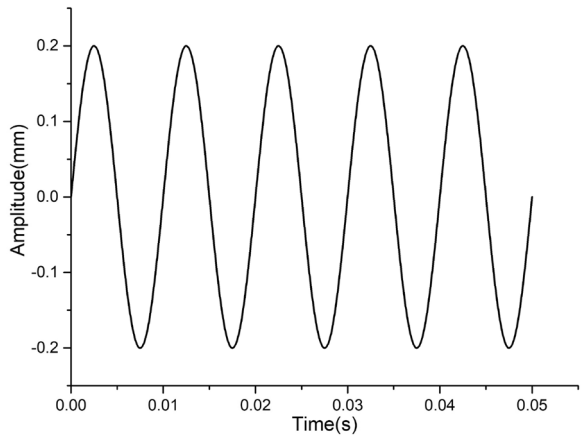

Figure 8 Excitation curve

curve representing the plunger's displacement over time, serving as a simulation of the excitation experienced by the tensioner due to chain fluctuations [24]. By introducing excitations of varied frequencies and amplitudes to the tensioner, its dynamic behavior under differing chain fluctuations can be effectively simulated.

The hydraulic tensioner primarily mitigates the chain's impact energy through the damping force, a viscous shear force produced by the interplay between the viscous medium and structural components. This action results in vibration and load reduction, ensuring that the chain load remains within an optimal range to guarantee the chain's fatigue life [25, 26]. Hence, the damping force is vital to the hydraulic tensioner's functionality. This research examined the impact of various leakage gaps, excitation amplitudes, oil temperatures, and air content levels on the tensioner's damping force. Concurrently, the study also explored how different leakage gaps affected chamber pressure and alterations in oil leakage.

3.2 Simulation Results

Hysteresis curves delineate the relationship between an output variable and both the current and historical values of an input variable. Originally applied to characterize the behavior of magnetic materials [27, 28], hysteresis curves have since gained prominence in hydraulic engineering [29, 30], particularly in addressing nonlinearity issues. In real-world applications, the hysteresis curve serves as a pivotal metric for gauging the efficacy of a tensioner, illustrating the interplay between displacement and damping force. The energy expended within one excitation cycle corresponds to the area encompassed by the hysteresis curve. A smoothly transitioning hysteresis curve with a substantial enclosed area indicates that the tensioner possesses considerable energy consumption and resilience against displacement excitation, aligning well with practical needs.

Figure 9 illustrates varied hysteresis curves based on distinct excitation amplitudes, given the following conditions: excitation frequency at 100 Hz, leakage gap at 0.035 mm, oil supply pressure at 0.4 MPa, oil temperature at 100 °C, and air content at 0.1%. From the figure, it is evident that the hydraulic tensioner's damping force increases with an increase in excitation amplitude. Specifically, for amplitude excitations of 0.05, 0.1, 0.15, and 0.2 mm, the maximum damping forces are 266.8, 544.4, 899.2, and 1086.3 N, respectively. Across varying amplitude excitations, the trend of the damping force of the tensioner remains consistent, and its smooth evolution underscores the tensioner's stable performance. As the hysteresis curve broadens, the encompassed area enlarges, signifying the enhanced energy absorption capacity of the tensioner. The curve's slight tilt relative to the y-axis stems from the tensioner's dynamic stiffness attributes and the influence of the leakage gap.

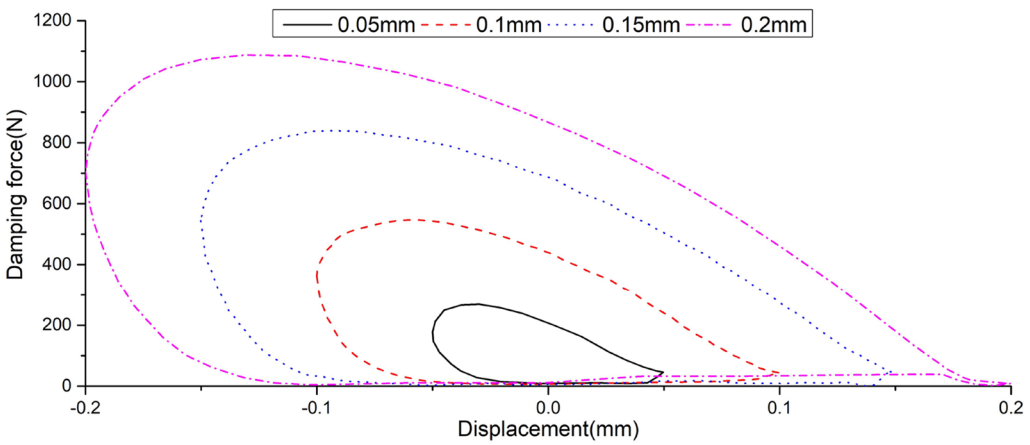

Figure 9 Damping forces for different excitation amplitudes

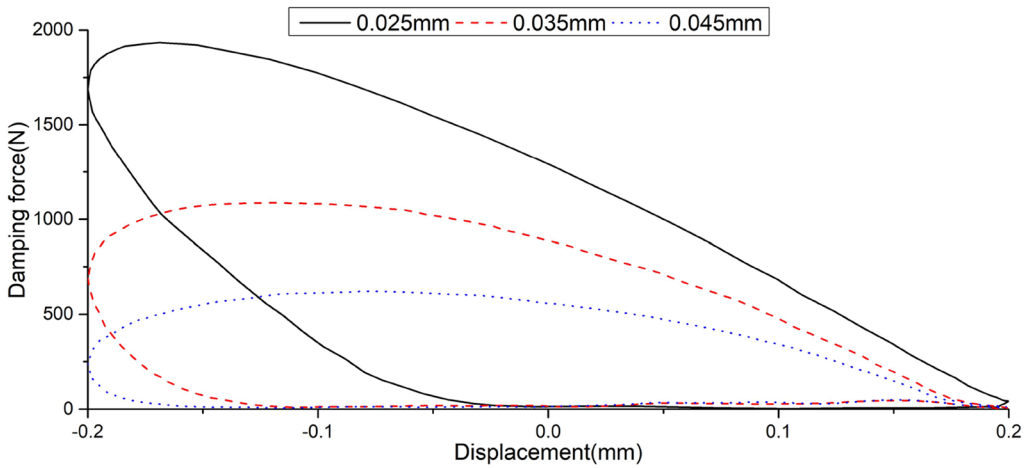

Figure 10 Damping forces for different leakage gaps

Figure 10 displays varied hysteresis curves corresponding to different leakage gaps, given the following conditions: excitation frequency at 100 Hz, excitation amplitude at 0.2 mm, oil supply pressure at 0.4 MPa, oil temperature at 100℃, and air content at 0.1%. For leakage gaps of 0.025, 0.035, and 0.045 mm, the maximum damping forces were measured at 1942.3, 1086.3, and 621.1 N, respectively. As evidenced by the results, a larger leakage gap results in a reduced damping force. Concurrently, the hysteresis curve narrows, its encompassed area shrinks, and the tensioner's energy absorption capability diminishes. These observations align with theoretical expectations. Thus, during the design phase, it is paramount to choose a suitable leakage gap based on the maximum tension of the chain's slack side, ensuring chain drive stability and minimizing noise.

Figure 11 presents varied hysteresis curves associated with different oil temperatures, considering the following conditions: excitation frequency at 100 Hz, excitation amplitude at 0.2 mm, leakage gap at 0.035 mm, oil supply pressure at 0.4 MPa, and air content at 0.1%. For oil temperatures of 80, 100, and 120 °C, the peak damping forces were 1634.1, 1086.3, and 792.8 N, respectively. As the temperature increases, there is a decline in oil viscosity. Consequently, the damping properties influenced by this oil viscosity weaken, leading to a reduction in the damping force of the tensioner. Therefore, it is essential to maintain the oil temperature within an optimal range during the tensioner's operational phase.

Figure 12 illustrates varied hysteresis curves for different air content levels, given the conditions: excitation frequency at 100 Hz, excitation amplitude at 0.2 mm, leakage gap at 0.035 mm, oil supply pressure at 0.4 MPa, and oil temperature at 100 °C. For air contents of 0.1%, 0.3%, and 0.5%, the peak damping forces were 1086.3, 1038.5, and 985.8 N, respectively. As the air content

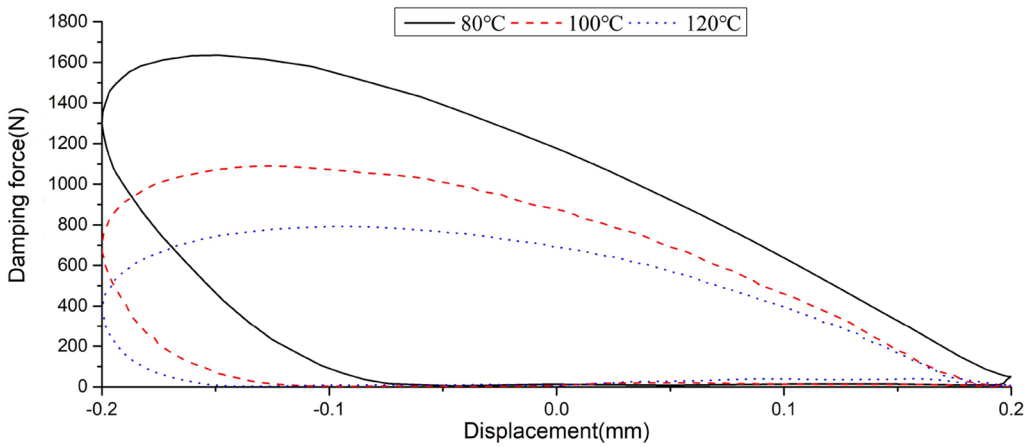

Figure 11 Damping forces at different temperatures

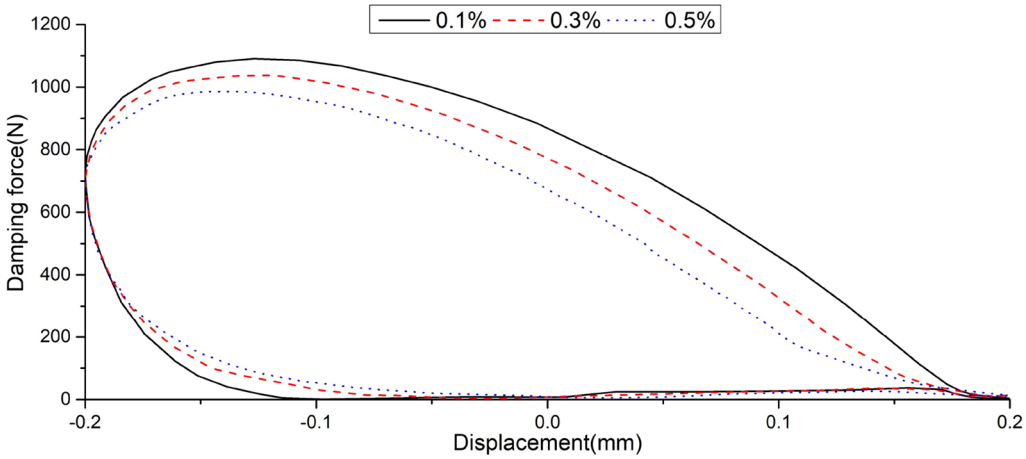

Figure 12 Damping forces for different air contents

within the oil rises, the damping force and envelope area gradually diminish. This decrease is attributed to the reduced bulk modulus as the air content increases in the viscous medium, leading to enhanced oil compressibility and weakened system damping characteristics. Consequently, the peak damping force drops. For an efficient hydraulic tensioner design, it is recommended to incorporate an exhaust port to consistently maintain low air content.

The oil pressure within the high-pressure chamber serves as a direct indication of the force the hydraulic tensioner conveys to the engine block. Figure 13 depicts varying pressure fluctuations in the high-pressure chamber based on different leakage gaps, adhering to the conditions: excitation frequency at 100 Hz, excitation amplitude at 0.2 mm, oil supply pressure at 0.4 MPa, temperature at 100 °C, and air content at 0.1%. The peak chamber pressures for leakage gaps of 0.025, 0.035, and 0.045 mm were 12.7, 7.6, and 4.3 MPa, respectively. The chart reveals a consistent decline in chamber pressure as the leakage gap expands. Furthermore, the chamber pressures for the different leakage gaps demonstrated a consistent pattern over time, sharing a similar trajectory.

Due to the presence of the leakage gap, a viscous damping force emerged to counter the chain's impact as oil exited the hydraulic tensioner. Figure 14 illustrates the varying leakage flows of the tensioner across different leakage gaps, considering conditions where the excitation frequency is 100 Hz, the excitation amplitude is 0.2 mm, the oil supply pressure stands at 0.4 MPa, the temperature is set at 100 °C, and the air content is 0.1%. The peak leakage flows for leakage gaps of 0.025, 0.035, and 0.045 mm were 9207, 14811, and 17533 mm^3/s, respectively. As the leakage gap expanded, the system's oil leakage

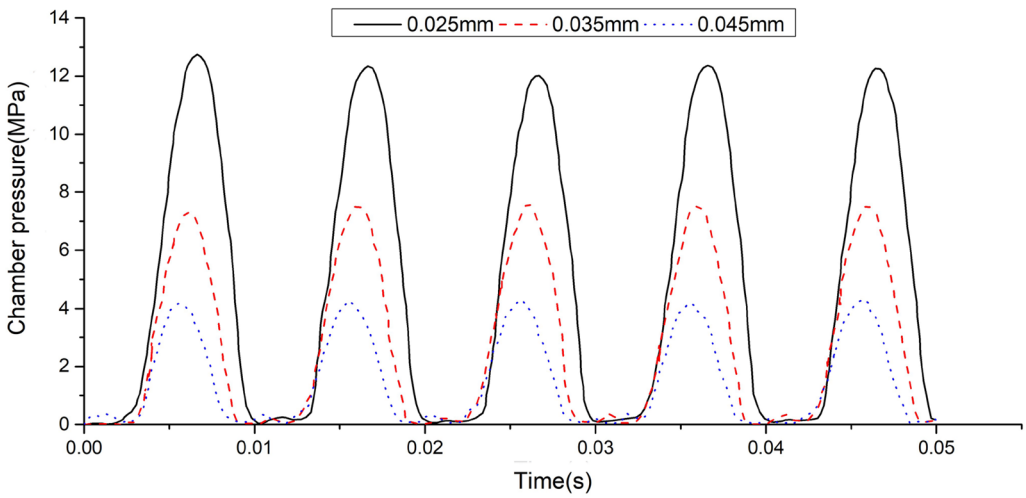

Figure 13 Chamber pressures for different leakage gaps

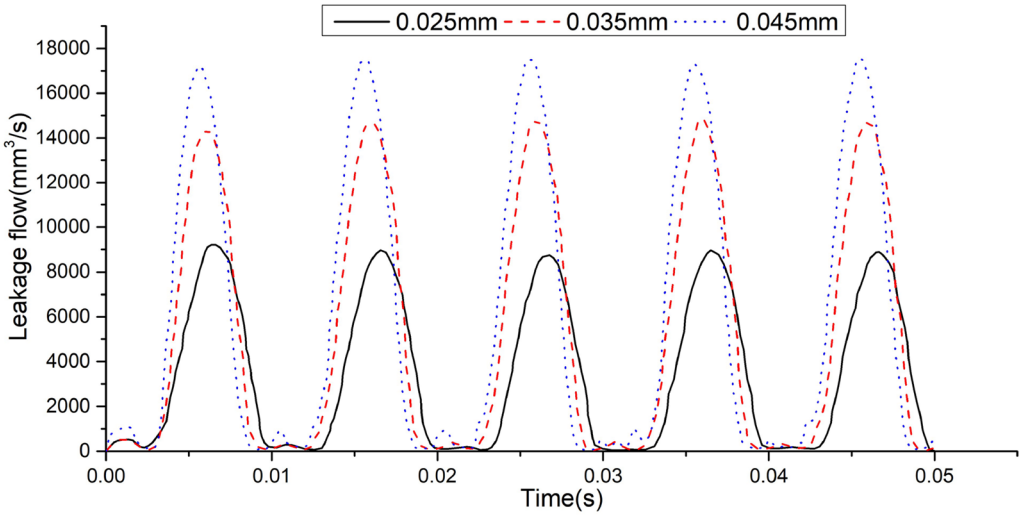

Figure 14 Oil leakage flows for different leakage gaps

intensified, undermining the tensioner's damping capabilities and leading to noise and vibrations in the timing system during its operation. Hence, it is crucial to select the right leakage gap based on the initial theoretical formula for oil flow at the beginning of the design.

4 Experimental Validation

4.1 Experimental Device

To assess the accuracy of the simulation outcomes, results from the calculations were compared with actual measurements. Experiments were conducted on the plunger reaction forces across varied excitation frequencies and amplitudes, maintaining the following conditions: a leakage gap of 0.035 mm, an oil supply pressure of 0.4 MPa, and an oil temperature of 100 °C. A sinusoidal excitation curve was employed for the tests. Figure 15 provides a diagram of the experimental apparatus. A hydraulic pump was used to deliver the necessary oil pressure, with the tensioner's oil supply pressure being adjusted through the relief valve. The temperature control unit set the maximum heating level, while a temperature sensor was employed to measure and relay feedback regarding the oil's temperature. A pressure sensor was tasked with determining the plunger reaction force, and a displacement sensor was used to record the plunger's movement. The data was recorded at a sampling frequency of 10 kHz. Figure 16 illustrates the testing equipment used for the hydraulic tensioner.

4.2 Comparison between Experimental and Simulation Results

Figure 17 examines the correlation between the reaction forces of the hydraulic tensioner and plunger's displacements under excitation frequencies of 50 and 100

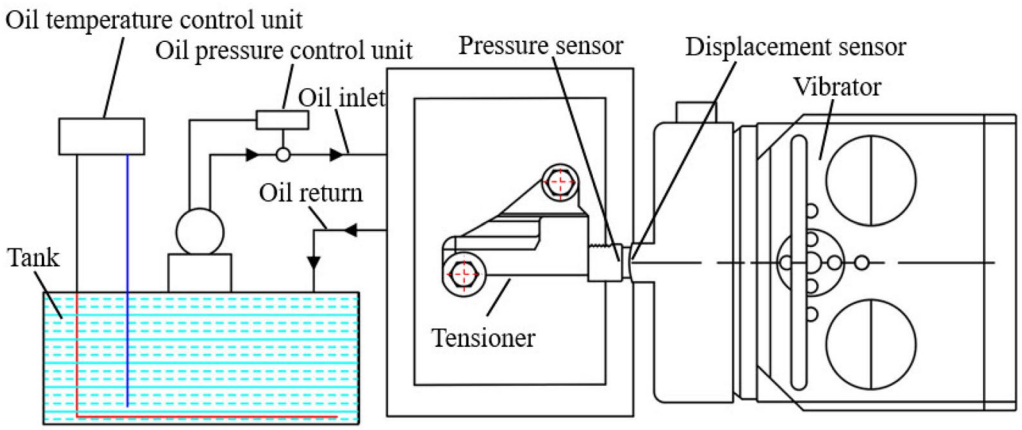

Figure 15 Schematic illustration of the experimental setup

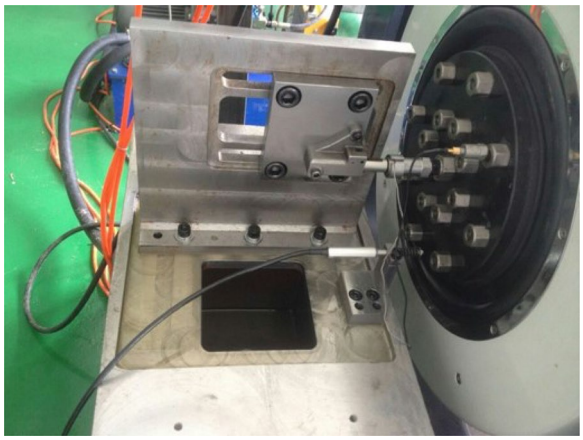

Figure 16 Test equipment for hydraulic tensioner

Hz. The comprehensive hysteresis curve suggests that the tensioner exhibits a high energy consumption profile under minimal displacement and robust impact resistance, aligning with the practical operational demands of hydraulic tensioners. The findings from the simulation closely mirror those from experimental tests, demonstrating a high degree of congruence at full amplitude.

Figure 18 illustrates the correlation between the maximum reaction force of the hydraulic tensioner and its frequency. The maximum reaction forces from both the simulation and experiment are outlined in Table 2. For amplitude excitations of 0.1, 0.15, and 0.2 mm, the disparities between the simulation and experimental results for the maximum reaction force are 81.6, 69.7, and 64.1 N, respectively. The prediction error for the maximum damping force across various excitation frequencies consistently stayed below 8.3%, which is deemed acceptable. The discrepancy is believed to mainly stem from uncertainties related to the air content in the hydraulic tensioner during testing. The oil's air content directly influences the tensioner's damping properties, as indicated in [18]. By introducing an air-leakage device at the plunger's location, the air content in the oil can be minimized. The graph reveals that the maximum reaction force follows a similar trajectory at each amplitude, peaking at around 150 Hz before declining.

A combined assessment of Figures 17 and 18 demonstrates that the simulation results align closely with the experimental findings, validating the simulation approach as an efficient means to anticipate the hydraulic tensioner's dynamic performance.

5 Conclusions

(1) Experimental findings validate the dynamic simulation analysis as a robust method to predict the hydraulic tensioner's dynamic behavior. The predicted error for the maximum damping force across varying excitation frequencies consistently remained below 8.3%. The primary source of this minor deviation can be attributed to uncertainties associated with the air content in the tested hydraulic tensioner.

(2) The behavior of the tensioner is significantly influenced by the size of the leakage gap. A narrower leakage gap leads to reduced oil flow and heightened chamber pressure, which in turn enhances the damping coefficient and expands the area of the hysteresis curve. Consequently, this results in a more substantial tensioner reaction force. As the leakage gap narrows from 0.045 to 0.025 mm, the maximum damping force increases from 621.1 to

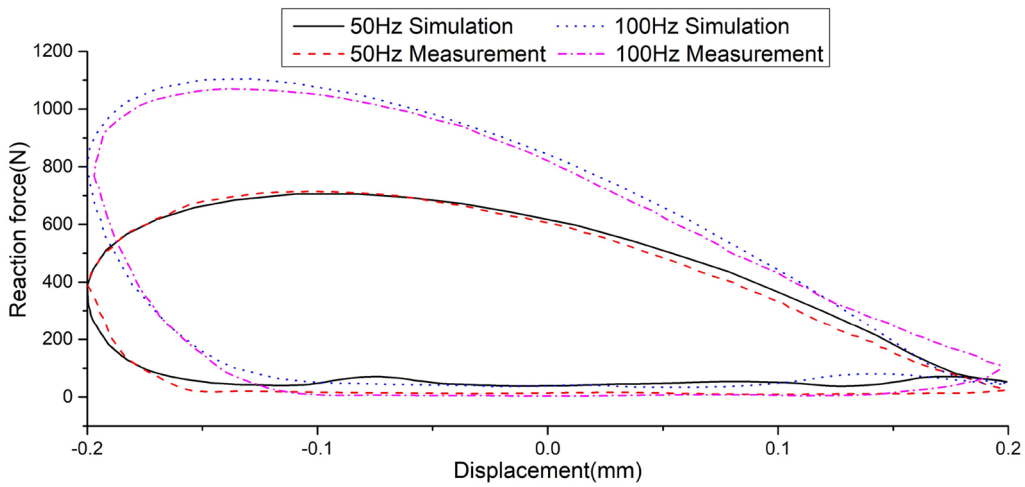

Figure 17 Reaction forces for different displacements of the plunger

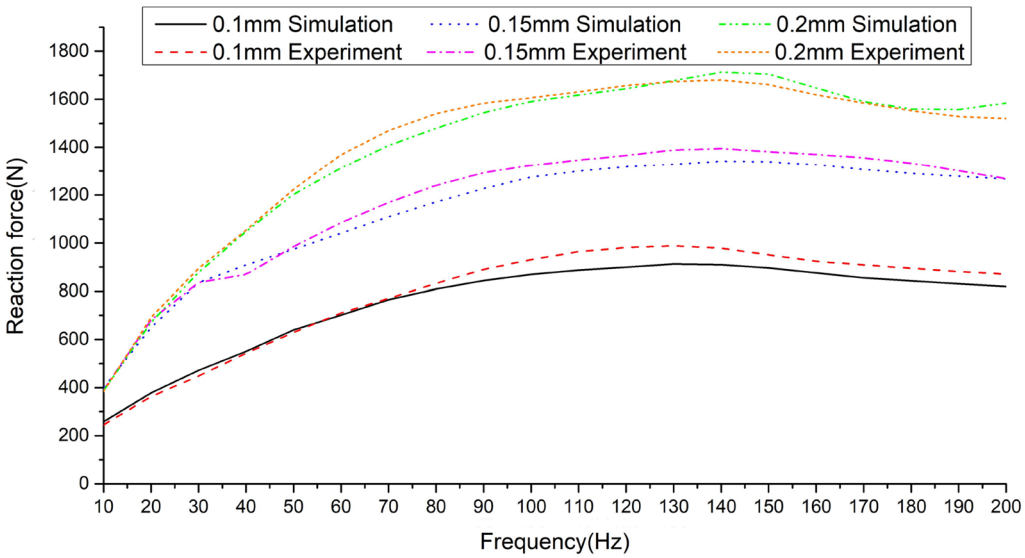

Figure 18 Reaction forces for different frequencies and amplitudes

Table 2 Maximum reaction forces for simulation and experiment

Excitation amplitude (mm)	Simulation (N)	Experiment (N)
0.1	912.4	988.4
0.15	1341.2	1394.7
0.2	1712.6	1680

1942.3 N. Therefore, during the preliminary design phase, it is crucial to determine the optimal leakage gap size, considering the tensioner's operational conditions and the insights gained from simulation results.

(3) As the oil temperature increases, its viscosity drops, leading to a decline in the peak damping force. Specifically, the damping force drops from 1634.1 to 792.8 N when the oil temperature rises from 80 to 120 °C. The presence of air in the hydraulic oil further diminishes the maximum damping force and contracts the area under the hysteresis curve. For instance, as the air content climbs from 0.1% to 0.3%, the damping force reduces from 1086.3 to 985.8 N. To optimize the performance of the hydraulic tensioner, it is essential to monitor the oil temperature and position the vent hole effectively to minimize the tensioner's air content.

Acknowledgements
Not applicable.

Author Contributions
ZF put forward the basic thought of design, simulation and experiments, and in charge of the whole trial. JY analysed simulation results and wrote the manuscript. FW assisted with modeling, data analyzing and manuscript. All authors read and approved the final manuscript.

Authors' Information
Zengming Feng, born in 1975, is currently a professor at *School of Mechanical and Aerospace Engineering, Jilin University, China*. He received his PhD degree from *Jilin University, China*, in 2006. His research interests include mechanical transmission and dynamic control, multi-body dynamic modeling and simulation, friction and wear.
Jinxing Yang, born in 1993, is currently PhD candidate at *School of Mechanical and Aerospace Engineering, Jilin University, China*. He received his master degree from *Jilin University, China*, in 2019.
Fei Wang, born in 1988, is currently a mechanical engineer at *Bosch Powertrain Co. LTD*. He received his master degree from *Jilin University, China*, in 2014.

Funding
Not applicable.

Data availability
The data that support the findings of this study are available from the corresponding author upon reasonable request.

Declarations

Competing Interests
The authors declare no competing financial interests.

Received: 16 January 2023 Revised: 5 September 2023 Accepted: 13 September 2023
Published online: 18 October 2023

References

[1] H Yu, L Zhao. Off-line simulation reaserch on vechicle turbocharger. *Electronic Design Engineering*, 2012, 20(1): 60-62. (in Chinese)
[2] J Wahlström, L Eriksson. Modelling diesel engines with a variable-geometry turbocharger and exhaust gas recirculation by optimization of model

parameters for capturing non-linear system dynamics. *Proceedings of the Institution of Mechanical Engineers, Part D: Journal of Automobile Engineering*, 2011, 225(7): 960–986.
[3] X Wang, H Zhao, H Xie. Effect of piston shapes and fuel injection strategies on stoichiometric stratified flame ignition (SFI) hybrid combustion in a PFI/DI gasoline engine by numerical simulations. *Energy Conversion & Management*, 2015, 98: 387–400.
[4] H Takagishi, A Nagakubo. Multi-Body dynamic chain system simulation using a blade tensioner. *SAE*, 2006-32-0067, 2006.
[5] J R Dwyer, R Lewis, A Ward, et al. Determination of impact stresses in an automotive chain drive component. *SAE*, 2006-01-0766, 2006.
[6] Z M Feng, F Z Meng, C T Li. The meshing mechanism and simulation analysis of a new silent chain. *Journal of Shanghai Jiaotong University*, 2005, 39(9): 1427-1430. (in Chinese)
[7] Y M Li, Z Y Hao, Z M Zhang, et al. Simulation research on dynamic characteristic of timing chain trains of gasoline engine. *Chinese Internal Combustion Engine Engineering*, 2013, 34(1): 81-86. (in Chinese)
[8] R Mulik, M Joshi, S Gajjal. Dynamic analysis of timing chain system of a high speed three cylinder diesel engine. *International Journal of Engineering and Science*, 2014, 4(5): 21-25.
[9] M Cali, G Sequenzia, S Oliveri. Meshing angles evaluation of silent chain drive by numerical analysis and experimental test. *Meccanica*, 2016, 51(3): 475-489.
[10] J X Yang, Z M Feng, X G Wang. Oil injection lubrication analysis of a silent chain drive system. *Advances in Engineering Software*, 2022, 172: 103210.
[11] T C Kraver, G W Fan, J Shah. Complex modal analysis of a flat belt pulley system with belt damping and coulomb-damped tensioner. *ASME 1994 International Computers in Engineering Conference and Exhibition*, 1994, 448: 589-595.
[12] G Michon, L Manin, R Dufour. Hysteretic behavior of a belt tensioner: modeling and experimental investigation. *Journal of Vibration and Control,* 2005, 11(9) :1147-1158.
[13] L Q Chen, Z Wei. Adaptive vibration reduction of an axially moving string via a tensioner. *International Journal of Mechanical Sciences*, 2006, 48(12): 1409-1415.
[14] W Podsiedlik, J Wojtysiak. Multi - barrier electromagnetic tensioner for control of yarn tension in processing. *Fibres & Textiles in Eastern Europe*, 2006, 14(5): 125-128.
[15] H Takagishi, K Muguruma, N Takahashi, et al. Analysis of effect of tensioner on chain system. *SAE*, 2008-01-1496, 2008.
[16] Y M Hu, L Q Han, J Liu, et al. Mathematical modeling and FEA verification for the damping characteristics of a hydraulic tensioner. *Automotive Engineering*, 2014, 36(2): 204-209. (in Chinese)
[17] X K Zeng, H Y Wang, J R Liu. Tests for dynamic characteristic of an automatic tensioner in an accessory drive system and its modelling. *Journal of Vibration and Shock*, 2014, 33(18): 149-155. (in Chinese)
[18] J X Xi, Z M Feng, G Q Wang, et al. Vibration and noise source identification methods for a diesel engine. *Journal of Mechanical Science and Technology*, 2015, 29(1): 181-189.
[19] M Sakaguchi, S Yamada, M Seki, et al. Study on reduction of timing chain friction using multi-body dynamics. *SAE*, 2012-01-0412, 2012.
[20] K Krueger, L Ginzinger, H Ulbrich. Influences of leakage gap variations on the dynamics of hydraulic chain tensioners – experiment and simulation. *SAE*, 2008-01-0294, 2008.
[21] H Gu, Y Ding. Effects of fluid compressibility on landing gear shimmy dampers. *Journal of Nanjing University of Aeronautics & Astronautics*, 1999, 31(6): 626-633. (in Chinese)
[22] M Qatu, M Dougherty, G Smid. Measurement of fluid bulk modulus using impedance of hydraulic circuits. *SAE,* 1999-01-0942, 1999.
[23] P Shi, Y Wang, L Wang. Study on modeling and simulation of the hydraulic fluid. *Transactions of the Chinese Society for Agricultural Machinery*, 2007, 38(12):148-151. (in Chinese)
[24] K Krueger, T Engelhardt, L Ginzinger, et al. Dynamical analysis of hydraulic chain tensioners - experiment and simulation. *SAE*, 2007-01-1461, 2007.
[25] O Polat, A Ebrinc, C Ozen, et al. Timing chain wear assessment with different type of oils. *SAE*, 2009-01-0198, 2009.
[26] P Shayler, A Allen, D Leong, et al. Characterising lubricating oil viscosity to describe effects on engine friction. *SAE*, 2007-01-1984, 2007.
[27] U Robels, J H Calderwood, G Arlt. Shift and deformation of the hysteresis curve of ferroelectrics by defects: An electrostatic model. *Journal of Applied Physics*, 1995, 77(8): 4002-4008.
[28] V Russier, C Petit, M P Pileni. Hysteresis curve of magnetic nanocrystals monolayers: Influence of the structure. *Journal of Applied Physics*, 2003, 93(12): 10001-10010.
[29] A Yu, Y Cheng, S Bhat. Evaluation of key hydraulic tensioner performance parameters for ultra deep water applications. *ASME International Conference on Offshore Mechanics and Arctic Engineering*, 2008, 27: 1-14.
[30] T Wang, Y Liu. Dynamic response of platform-riser coupling system with hydro-pneumatic tensioner. *Ocean Engineering*, 2018, 166(15): 172-181.